


FULL PAPER

Open Access



Simultaneous electrical resistivity and elastic wave velocity measurements during triaxial deformation of granite under brine-saturated conditions

Ikuo Katayama^{1*} , Yu Aoi¹, Kazumasa Tanimoto¹, Yuya Akamatsu¹ and Kazuki Sawayama²

Abstract

We report the first experiments, where simultaneous electrical resistivity and elastic wave velocity measurements are acquired during the triaxial deformation of granite under brine-saturated conditions. Both the resistivity and elastic wave velocity increase slightly during the early stage of deformation owing to crack closure, and then decrease systematically owing to crack development as the sample approaches failure. We observe a complex relationship among the resistivity, elastic wave velocity, and porosity during deformation that is likely attributed to their different sensitivities to crack orientation, tortuosity, and connectivity. The electrical resistivity changes tend to decline as the sample approaches failure owing to the nearly complete crack connectivity, whereas the elastic wave velocities continue to decrease. These characteristic changes in resistivity and velocity at the discrete stages of deformation may provide a clue to understanding structural changes in crystalline basements that are related to crack development and fluid infiltration.

Keywords Electrical resistivity, Elastic wave velocity, Deformation, Crack, Granite

*Correspondence:

Ikuo Katayama

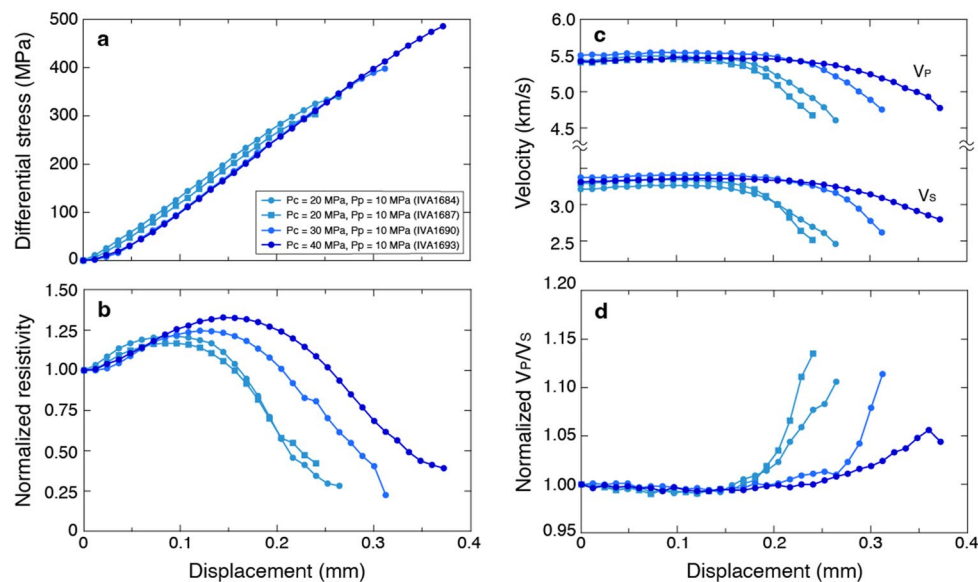
katayama@hiroshima-u.ac.jp

Full list of author information is available at the end of the article



© The Author(s) 2023. **Open Access** This article is licensed under a Creative Commons Attribution 4.0 International License, which permits use, sharing, adaptation, distribution and reproduction in any medium or format, as long as you give appropriate credit to the original author(s) and the source, provide a link to the Creative Commons licence, and indicate if changes were made. The images or other third party material in this article are included in the article's Creative Commons licence, unless indicated otherwise in a credit line to the material. If material is not included in the article's Creative Commons licence and your intended use is not permitted by statutory regulation or exceeds the permitted use, you will need to obtain permission directly from the copyright holder. To view a copy of this licence, visit <http://creativecommons.org/licenses/by/4.0/>.

Graphical Abstract



Introduction

The electrical resistivity and elastic wave velocity of rocks are sensitive to the presence of both cracks and fluids, such that these physical properties are frequently used to investigate structural changes in the crust (e.g., Scholz et al. 1973; Nimiya et al. 2017; Minami et al. 2018). Laboratory experiments can monitor microcrack formation due to brittle deformation based on changes in electrical resistivity (e.g., Brace and Orange 1968; Tomecka-Suchon and Rummel 1992; Glover et al. 2000) and elastic wave velocity (e.g., Hadley 1975; Lockner et al. 1977; Schubnel et al. 2003; Fortin et al. 2011). However, simultaneous electrical resistivity and elastic wave velocity measurements are rarely obtained during the triaxial deformation of crystalline rocks. Although both of these properties are sensitive to crack closure and development, they exhibit different sensitivities to cracks. The electrical resistivity is controlled mainly by fluid channels, such that it is highly dependent on the connectivity and networking of fluid-filled cracks, whereas the elastic wave velocities are mainly affected by the number and size of cracks (i.e., crack density) as the elastic waves pass through the rock (e.g., Guéguen and Palciauskas 1994; Paterson and Wong 2005). Pioneer work by Watanabe and Higuchi (2015) has measured both the resistivity and velocity of granite during hydrostatic compression, and they demonstrated that a close correlation exists between these properties; however, the crack orientation is nearly random in their

hydrostatic experiments, whereas anisotropic crack development is expected during triaxial deformation.

We have systematically measured the elastic wave velocities (compressional and shear wave velocities; V_P and V_S , respectively) during the triaxial deformation of various rocks under dry and fluid-saturated conditions in the laboratory (e.g. Zaima and Katayama 2018; Akamatsu et al. 2021). In this study, we have further improved the experimental system to successfully conduct simultaneous electrical resistivity and elastic wave velocity measurements during triaxial deformation under brine-saturated conditions (Fig. 1). Furthermore, the sample porosity can be inferred from the change in fluid volume of the reservoir, which is simultaneously monitored during the experiments. Here, we employ these data to discuss the relationship among the electrical resistivity, elastic wave velocities, and porosity with respect to crack closure and development during the deformation of granitic rock, and their application to geological phenomena.

Experimental methods

Laboratory experiments were conducted on Aji granite (Kagawa, Japan), which is mainly composed of quartz, plagioclase, potassium-feldspar, and biotite, with a mean grain size of 0.5 mm. The samples were characterized by a low initial porosity (~0.8%) and negligible anisotropy. Cylindrical samples of 20 mm diameter and 40 mm length were prepared, with the ends of the cylinders

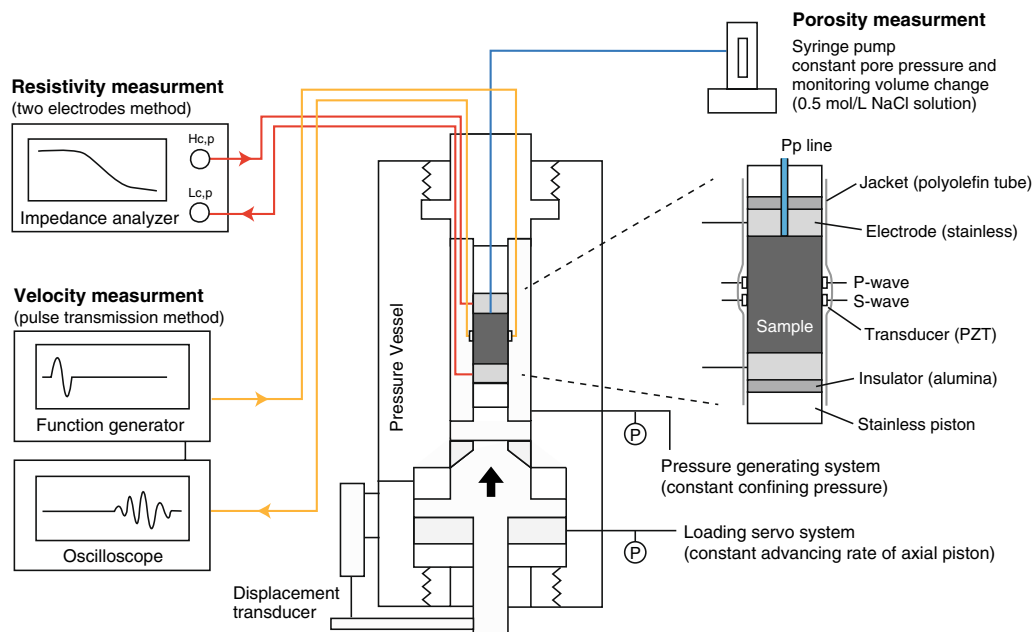


Fig. 1 Schematic diagram showing the experimental apparatus and simultaneous measurement system for electrical resistivity, elastic wave velocity, and porosity. Sample is sandwiched by two electrodes, which are electrically isolated by the alumina insulator, and piezoelectric transducers are directly attached to the sample

ground flat and parallel to each other. All of the samples were dried in a vacuum oven at 100 °C for > 24 h before the experiments.

Triaxial deformation experiments were performed using the intra-vessel deformation and fluid-flow apparatus at Hiroshima University, Japan (e.g., Zaima and Katayama 2018; Akamatsu et al. 2021). Each sample was saturated with brine (0.5 mol/L NaCl solution, 0.24 Ωm) for > 24 h after installing the assembly into the pressure vessel until the fluid volume in the reservoir and the electrical resistivity of the sample became both stationary. The axial piston was then advanced at a constant displacement rate of 0.0015 mm/min (strain rate of $6 \times 10^{-7} \text{ s}^{-1}$) at a given confining pressure, which ranged

system to compensate for the advanced piston volume into the pressure vessel. The pore pressure was kept constant using a syringe pump ($P_p = 10 \text{ MPa}$), and the fluid volume was monitored to calculate the porosity changes due to crack closure and development during deformation. The detailed experimental conditions are shown in Table 1.

The elastic wave velocities were determined via the pulse transmission method, whereby the travel times of the elastic wave through the sample were measured using a piezoelectric transducer with a resonant frequency of 2 MHz. The transducers were attached directly to the sample surface to make the propagation direction normal to the vertical compression axis, and the shear-wave was

Table 1 Experimental samples and conditions

Run number	Density (g/cm ³)	Porosity (%)	Confining pressure (MPa)	Pore pressure (MPa)	Strain rate (s ⁻¹)	Maximum stress (MPa)
IVA1684	2.65	0.63	20	10	6×10^{-7}	285
IVA1687	2.64	0.81	20	10	3×10^{-7}	322
IVA1690	2.65	0.70	30	10	6×10^{-7}	284
IVA1693	2.64	0.80	40	10	6×10^{-7}	295

from 20 to 40 MPa. A constant confining pressure was maintained during deformation using a servo-controlled

polarized in the horizontal plane (see Zaima and Katayama (2018) for further detail). The electrical resistivity

was determined via a two-electrode method, whereby the sample was sandwiched between two stainless electrodes in the direction parallel to the compression axis. The direction of the resistivity measurements was different to those of the elastic wave velocities; however, the directions of both measurements were sensitive to the vertical cracks, aligned parallel to the compressional axis, which yield a relatively short effective channel length. The sample impedances were measured at the frequency from 20 Hz to 1 MHz using an impedance analyzer (Keysight Technologies E4990A). Figure 2 shows the impedance spectra and Cole–Cole plots of a series of deformation experiment (IVA1684). The Cole–Cole plots yielded a single arc, indicating a dominant role of pore fluid, with a slight distortion at low frequencies most likely due to the inductance effects. The impedance spectra were well-reproduced by the RCL circuits with a parallel connection of the resistance, capacitance, and inductance, but the slight deviation indicates a more complex electrical conduction path operated in our experimental system (Additional file 1: Fig. S1). Therefore, we used the 1 kHz data to estimate the sample resistivity, where the spectra exhibited a plateau impedance value with a small phase shift. The experiments were conducted at room temperature, and we applied a temperature correction to the resistivity using a correction factor of 0.02/ °C that was normalized to 20 °C (Revil et al. 1998). We recorded the elastic wave velocities (V_p and V_s) and electrical resistivity at each 0.012 mm displacement step. Although a short time gap existed between the elastic wave velocity and impedance measurements (~ 30 s), the difference was almost negligible because of the relatively slow strain rate during our experiments.

Electrical resistivity and elastic wave velocity changes during deformation

The stress–displacement (strain) curves of the granite samples during triaxial deformation are shown in Fig. 3a, and the results are summarized in Table 2. The maximum stress achieved during deformation varies from 303 to 486 MPa, with the samples deformed at high confining pressure yielding a higher differential stress. The stress dropped abruptly after the peak stress when the rock specimen began to fail in our constant loading-rate experiments, such that no electrical resistivity and elastic wave velocity measurements were made during the post-failure stage.

The electrical resistivity changes during deformation are shown in Fig. 3b, whereby the resistivity is normalized to the initial value prior to deformation. The resistivity tends to increase during the initial loading stage, and then decreases systematically until failure occurs. This transition from an increase to a decrease

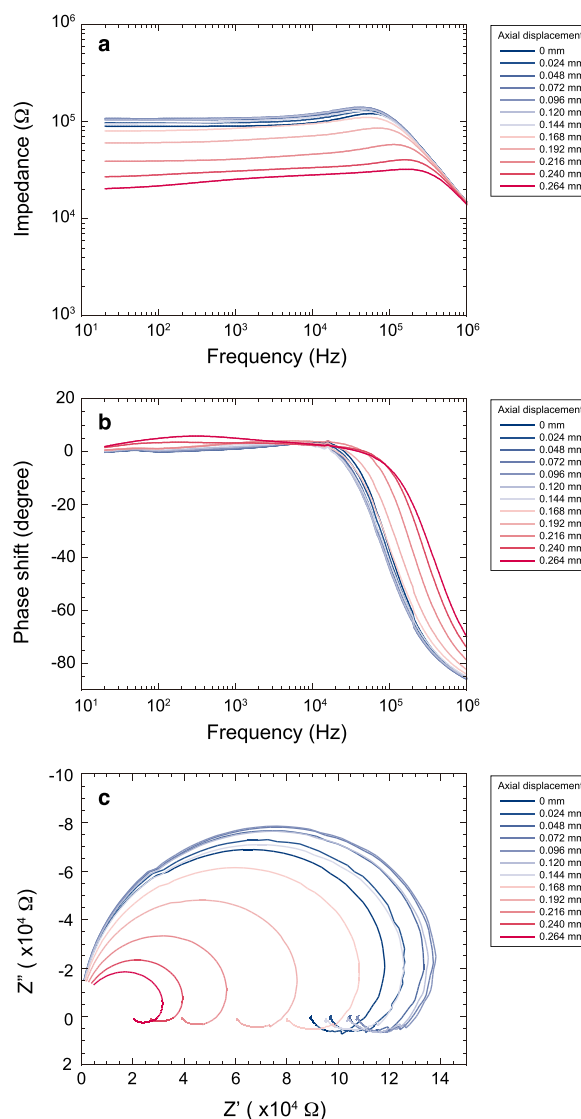


Fig. 2 Impedance spectra recorded during deformation experiment of IVA1684. **a** Amplitude of impedance $|Z|$ as a function of frequency. **b** Phase shift as a function of frequency. **c** Cole–Cole plots showing real (Z') and imaginary (Z'') parts of complex impedance

in resistivity occurs at approximately 40% of the maximum stress for each sample and largely coincides with the increase of porosity (Fig. 4), which agrees with the onset of dilatancy identified using strain measurements during triaxial deformation of the same material (Sawayama and Katayama 2016). A similar concave-down evolution of the electrical resistivity during the deformation of granite has been reported in previous experiments (Brace and Orange 1968; Tomecka-Suchon and Rummel 1992), even though different strain rates, confining pressures, and pore fluid pressures were employed. At higher effective pressures, the

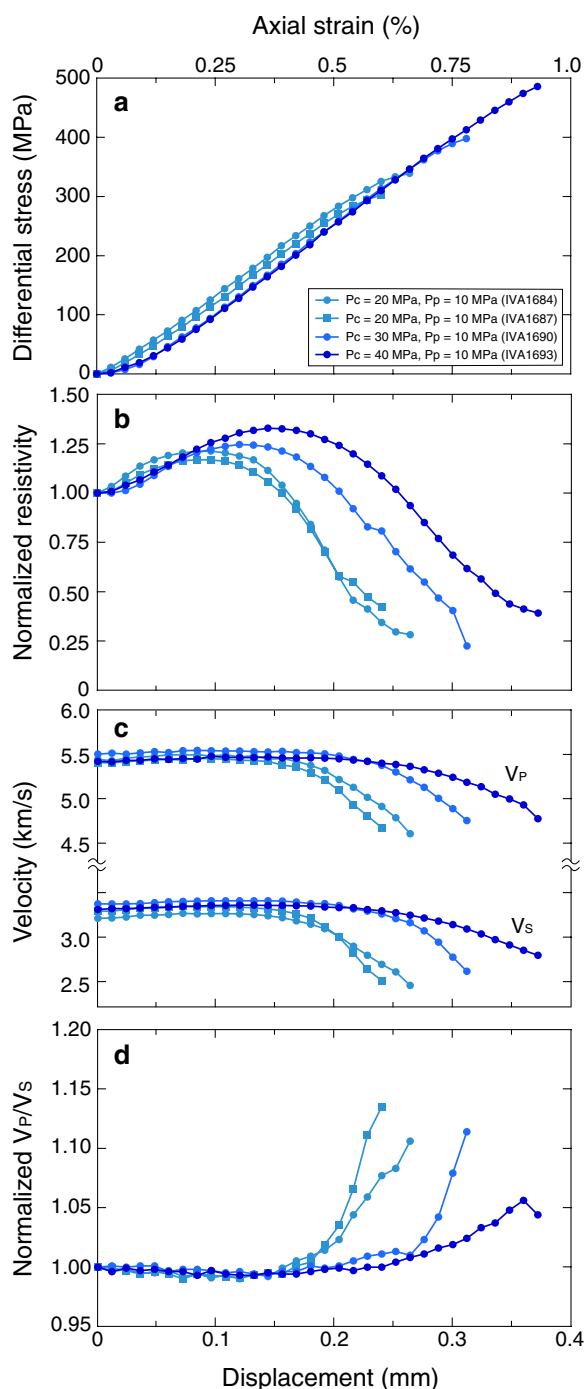


Fig. 3 **a** Stress and displacement curves for the experiments under brine-saturated conditions. The axial strain, which is inferred from the displacement, is also shown on the upper axis. **b** Electrical resistivity changes during deformation, which are normalized to the initial value prior to deformation. **c** Elastic wave velocity (V_p and V_s) changes during deformation. **d** V_p/V_s changes during deformation, which are normalized to the initial value prior to deformation

increase in resistivity during the early stage is larger due to the effective compaction, but the overall evolution of resistivity is similar among the experiments at different confining pressures. We conducted a deformation experiment at a slow strain rate ($3 \times 10^{-7} \text{ s}^{-1}$), and the results were almost identical to those obtained at the same effective pressure, which indicates that the fluid supply into the specimen was sufficient during deformation.

Figure 3c, d highlights the elastic wave velocities and V_p/V_s changes, respectively, during deformation. Both V_p and V_s increase slightly during the initial stage of deformation and then decrease significantly during the later stage of deformation until failure occurs. The results are similar to the previous experiments using the same material (Zaima and Katayama 2018) and other granitic rocks (e.g. Hadley 1975; Lockner et al. 1977; Schubnel et al. 2003). V_p/V_s remains nearly constant during the initial loading, but then increases significantly during the later stage of deformation. This is consistent with the development of cracks that are filled with an aqueous fluid, whereas dry cracks undergo a decrease in V_p/V_s based on effective medium theory (e.g. O’Connell and Budiansky 1974; Kachanov 1994). At higher confining pressures, the changes in velocities are slightly suppressed most likely due to the inhibition of crack formation.

These electrical resistivity and elastic wave velocity changes correspond to porosity change in the samples, with the decreases in resistivity and velocity beginning once the samples are placed approximately half of the fracture stress and the rock becomes dilatant (Fig. 4). The rapid decreases in resistivity and velocity, as well as the increase in V_p/V_s , as the samples approach failure are accompanied by a rapid increase in porosity. This notable relationship among the electrical resistivity, elastic wave velocities, and porosity indicates that these properties are controlled mainly by crack closure and development in the rock specimens. This behavior is consistent in all of the experiments at different confining pressures in the 20–40 MPa range and in agreement with previous experiments that were conducted at pressures up to 550 MPa (Brace and Orange 1968), suggesting that pressure does not have a dominant influence on the evolution of the electrical resistivity and elastic wave velocity during the deformation of granitic rocks under conditions studied here. At much higher pressure and especially coupled with temperature, granite will show ductility and the evolution of these properties will be very different, as indicated by Violay et al. (2017).

Table 2 Experimental results of resistivity, elastic wave velocities, and porosity during deformation

Displacement (mm)	IVA1684				IVA1687				IVA1690				IVA1693			
	Resistivity (Ohm m)	V_p (km/s)	V_s (km/s)	Porosity (%)	Resistivity (Ohm m)	V_p (km/s)	V_s (km/s)	Porosity (%)	Resistivity (Ohm m)	V_p (km/s)	V_s (km/s)	Porosity (%)	Resistivity (Ohm m)	V_p (km/s)	V_s (km/s)	Porosity (%)
0	796	5.44	3.21	0.548	634	5.41	3.29	0.773	1113.2	5.5	3.37	0.62	1027.1	5.42	3.31	0.71
0.012	822.5	5.43	3.22	0.536	639.6	5.4	3.29	0.725	1112.5	5.51	3.37	0.63	1035.3	5.42	3.32	0.72
0.024	864.1	5.46	3.23	0.525	665.2	5.42	3.31	0.711	1127.3	5.5	3.37	0.6	1066.8	5.43	3.32	0.71
0.036	905.3	5.47	3.24	0.501	693.1	5.43	3.32	0.679	1161.6	5.52	3.38	0.59	1096.4	5.43	3.33	0.7
0.048	930.1	5.48	3.25	0.464	712.7	5.44	3.32	0.691	1211.5	5.53	3.39	0.57	1136.3	5.45	3.33	0.69
0.06	947.2	5.49	3.25	0.465	725.4	5.44	3.33	0.672	1263.2	5.52	3.4	0.56	1171.9	5.44	3.34	0.68
0.072	958	5.49	3.27	0.473	737.8	5.44	3.34	0.648	1307.6	5.54	3.4	0.55	1213.5	5.45	3.35	0.66
0.084	963.7	5.5	3.26	0.451	741.3	5.46	3.34	0.663	1338.8	5.55	3.41	0.55	1255.7	5.45	3.35	0.65
0.096	965	5.48	3.26	0.436	740.3	5.45	3.34	0.639	1360.6	5.54	3.41	0.55	1288.7	5.48	3.36	0.66
0.108	958	5.5	3.27	0.435	735.5	5.45	3.34	0.637	1376.9	5.54	3.41	0.53	1312.3	5.47	3.36	0.65
0.12	946.1	5.47	3.26	0.448	723.3	5.44	3.34	0.653	1386.5	5.54	3.41	0.55	1340.6	5.46	3.36	0.64
0.132	930.5	5.48	3.25	0.454	701	5.43	3.33	0.64	1383.5	5.53	3.41	0.55	1353.9	5.46	3.36	0.64
0.144	887.5	5.45	3.24	0.46	670	5.42	3.32	0.655	1372.8	5.53	3.41	0.52	1364.9	5.47	3.36	0.62
0.156	827.2	5.45	3.22	0.467	632.5	5.38	3.3	0.654	1350.1	5.54	3.41	0.53	1362.1	5.46	3.36	0.63
0.168	753.7	5.42	3.18	0.467	581.6	5.36	3.26	0.657	1315.9	5.52	3.4	0.55	1352.3	5.46	3.35	0.63
0.18	668.9	5.38	3.14	0.493	518.5	5.29	3.21	0.69	1263	5.52	3.38	0.55	1334.9	5.46	3.35	0.62
0.192	565.7	5.32	3.09	0.534	443.4	5.21	3.12	0.722	1202.6	5.51	3.38	0.52	1306.3	5.46	3.34	0.63
0.204	456.2	5.22	3.01	0.56	366.9	5.09	3	0.814	1122.8	5.48	3.36	0.55	1274.9	5.45	3.33	0.64
0.216	363.2	5.13	2.9	0.649	347.3	4.93	2.82	0.95	1024.6	5.44	3.32	0.57	1230.3	5.44	3.33	0.64
0.228	326.8	5.02	2.79	0.721	299	4.81	2.63	1.081	922	5.42	3.29	0.6	1176.8	5.42	3.31	0.65
0.24	273.1	4.91	2.69	0.866	266.6	4.67	2.51	1.286	899.3	5.38	3.26	0.63	1116	5.4	3.3	0.63
0.252	235.8	4.78	2.61	1.015	-	-	-	-	782	5.3	3.21	0.64	1045.9	5.39	3.28	0.66
0.264	224.5	4.6	2.46	1.175	-	-	-	-	685	5.21	3.16	0.68	962.1	5.36	3.25	0.65
0.276	-	-	-	-	-	-	-	-	610.3	5.13	3.07	0.75	873.2	5.33	3.22	0.69
0.288	-	-	-	-	-	-	-	-	520.6	5	2.94	0.84	789.8	5.29	3.18	0.74
0.3	-	-	-	-	-	-	-	-	449.7	4.89	2.78	0.94	703.9	5.24	3.14	0.73
0.312	-	-	-	-	-	-	-	-	250	4.75	2.62	1.15	633.7	5.18	3.09	0.76
0.324	-	-	-	-	-	-	-	-	-	-	-	-	580.4	5.13	3.03	0.81
0.336	-	-	-	-	-	-	-	-	-	-	-	-	505.5	5.05	2.97	0.85
0.348	-	-	-	-	-	-	-	-	-	-	-	-	449.7	5	2.91	0.91
0.36	-	-	-	-	-	-	-	-	-	-	-	-	423.6	4.93	2.85	0.97
0.372	-	-	-	-	-	-	-	-	-	-	-	-	402.1	4.78	2.79	1.04

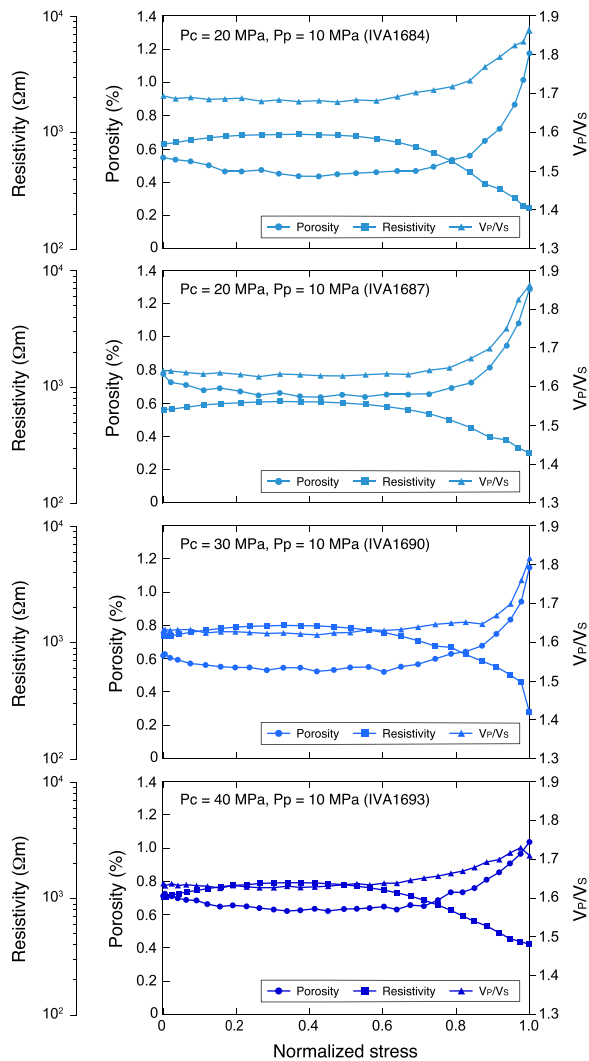


Fig. 4 Electrical resistivity, porosity, and V_p/V_s changes as a function of stress, which are normalized to the maximum stress during the deformation of each sample

Discussion

We have shown that the change in electrical resistivity is closely related to the change in porosity due to crack

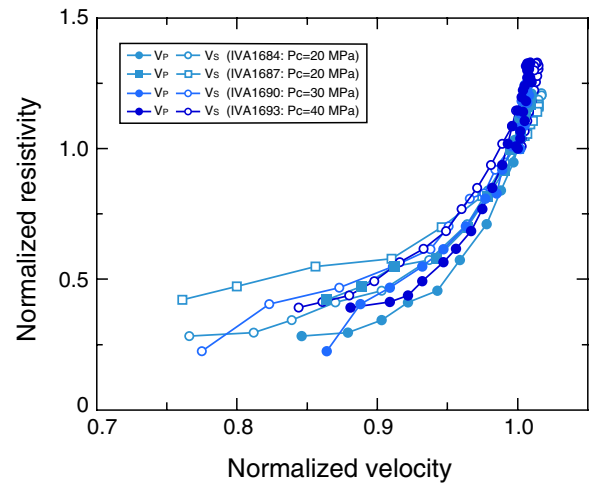


Fig. 6 Relationship between the electrical resistivity and elastic wave velocities during the deformation experiments, with both measurements normalized to their initial values prior to deformation

closure and development during deformation, and that these cracks are fully saturated based on elastic wave velocities. The relationship between the electrical resistivity and fluid-filled porosity is commonly described by Archie’s law:

$$\rho_s = \rho_f \phi^{-m}$$

where ρ_s is the resistivity of the sample, ρ_f is the resistivity of the pore fluid, ϕ is the porosity, and m is the cementation factor (e.g., Guéguen and Palciauskas 1994). The cementation factor for crystalline rocks, such as granite, has been reported to be approximately $m=2$ during hydrostatic compressional tests (Brace et al. 1965), whereas dilatancy-related crack development during brittle deformation has yielded $m=1$ (Brace and Orange 1968). Figure 5 shows the relationship between the electrical resistivity and porosity in this study. The resistivity and porosity slopes are different between the compaction and dilation stages, with a larger m exponent often observed during the early stage of dilation. These

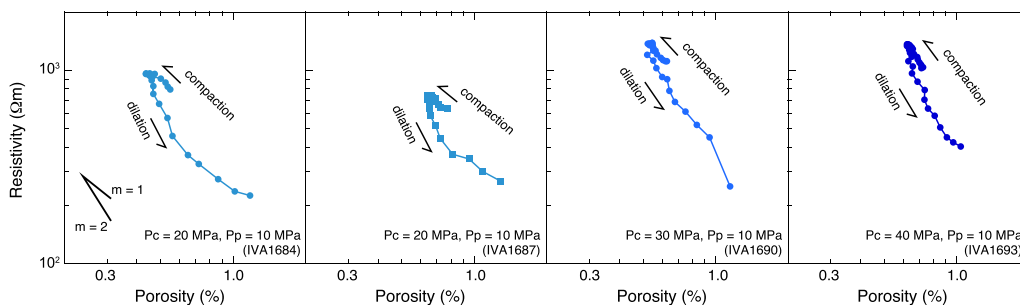


Fig. 5 Relationship between the electrical resistivity and porosity during the deformation of each sample, with the different trends between compaction and dilation caused by crack closure and development shown

complex behaviors cannot be explained by the Archie's relationship. The equivalent channel model introduces the electrical tortuosity that relates to the efficiency of electrical flow paths (Walsh and Brace 1984). As cracks are developed during the dilation stages, the crack interaction and connection result in decreasing tortuosity, which likely enhanced the electrical transmissibility through the samples.

The change of electrical resistivity during deformation is also attributed to the crack orientation. The initial cracks that are normal to the compressional axis (horizontal cracks) tend to close during the early stage of deformation, when the samples undergo compaction, although dilation occurs due to the developed cracks that are aligned parallel to the compressional axis (vertical cracks). These features have been well-reconciled by multi-component measurements of the elastic wave velocities and their tensor analysis, in which the horizontal cracks closed at the early stage of deformation and the vertical cracks developed during the later stage of deformation until failure occur (e.g. Schubnel et al. 2003; Fortin et al. 2011; Akamatsu et al. 2021). The electrical resistivity was measured in the direction parallel to the compressional axis, such that the effective channel length can be markedly small for the developments of vertical cracks in the measurement direction. The different tortuosity depending on the crack orientation may account for the different relationship between the resistivity and porosity during brittle deformation. The dependence of resistivity upon porosity diminishes during the later stage of deformation, when the samples are close to failure (Fig. 5). This behavior is likely due to the high crack density above the percolation threshold, when the sample approaches to failure, electrical resistivity becomes highly sensitive to the crack porosity but less sensitive to their connectivity (e.g., Guéguen and Dienes 1989). The changes in resistivity mostly agree with the permeability evolutions during triaxial compression; however, permeability showed a rapid increase at close to failure, because it is highly sensitive to hydraulic aperture (e.g., Mitchell and Faulkner 2008; Faoro et al. 2013).

Electrical resistivity and seismic velocity have often been employed to investigate structural changes in the crust. The earthquake physical model proposed by Scholz et al. (1973) is based on the changes in physical properties prior to earthquake that are related to dilatancy and water diffusion. Although this model has not yet been validated because of the general absence of precursor anomalies in the geological scale (e.g., Jordan et al. 2011), laboratory experiments have shown systematic changes in the physical properties of the deformed rock related to brittle deformation (e.g.,

Paterson and Wong 2005). Here, we demonstrated that both the electrical resistivity and elastic wave velocities undergo systematic changes during brittle deformation until failure occurs, and that their relationship is not sensitive to the choice of the confining pressure (Fig. 6). Our experimental results show a marked variation in electrical resistivity relative to the velocity; however, the resistivity becomes less sensitive to crack development as the sample approaches failure owing to the nearly complete connectivity of the crack networks. These characteristic changes in resistivity and velocity at discrete deformation stages may provide a clue for detecting structural changes prior to the generation of giant earthquakes. The electrical resistivity and elastic wave velocities are also dependent on the fluid saturation, whereby the resistivity and V_p/V_S are expected to decrease if the cracks are not filled with aqueous fluids. Note that crack orientation is sensitive to the stress fields, such that the measurement direction influences the changes of these physical properties. These unique characteristics and their applicability in joint inversions are also useful for geophysical exploration, including geothermal and hydrocarbon exploration (e.g., Muñoz et al. 2010).

Supplementary Information

The online version contains supplementary material available at <https://doi.org/10.1186/s40623-023-01809-4>.

Additional file 1: Figure S1. a Assumed RCL circuit with a parallel connection of resistance (R1, R2), capacitance (CPE), and inductance (L). **b** Fitting result of the impedance data prior to deformation of IVA1684.

Acknowledgements

We thank Dr. Tohru Watanabe for technical advice during the resistivity measurements. We also thank two anonymous reviewers for their constructive comments.

Author contributions

IK planned the project. YA and KT conducted the experiments, and YA, IK, YA, and KS analyzed the data. All of the authors discussed the results and implications and approved the final version of the manuscript. All authors read and approved the final manuscript.

Funding

This research was supported by JSPS KAKENHI Grant Number 20H00200, 18H03733, and 16H06476 in Scientific Research on Innovative Areas "Science of Slow Earthquakes".

Availability of data and materials

Data sharing is not applicable to this article as all data are listed in Table 2. Please contact the author for any requests.

Declarations

Competing interests

The authors declare that they have no competing interests.

Author details

¹Department of Earth and Planetary Systems Science, Hiroshima University, Higashi-Hiroshima, Hiroshima 739-8526, Japan. ²Institute for Geothermal Sciences, Kyoto University, Beppu, Oita 874-0903, Japan.

Received: 12 July 2022 Accepted: 21 March 2023

Published online: 12 April 2023

References

- Akamatsu Y, Katayama I, Tonegawa T (2021) Changes in elastic wave velocity during brittle deformation of gabbro and peridotite: Implications for oceanic Moho reflectivity. *Earth Planet Sci Lett*. <https://doi.org/10.1016/j.epsl.2021.117036>
- Brace WF, Orange AS (1968) Electrical resistivity changes in saturated rocks during fracture and frictional sliding. *J Geophys Res* 73:1433–1445. <https://doi.org/10.1029/JB073i004p01433>
- Brace WF, Orange AS, Madden TR (1965) The effect of pressure on the electrical resistivity of water-saturated crystalline rocks. *J Geophys Res* 70:5669–5678. <https://doi.org/10.1029/JZ070i022p05669>
- Faoro I, Vinciguerra S, Marone C, Elsworth D, Schubnel A (2013) Linking permeability to crack density evolution in thermally stressed rocks under cyclic loading. *Geophys Res Lett* 40:2590–2595. <https://doi.org/10.1002/grl.50436>
- Fortin J, Stanchits S, Vinciguerra S, Guéguen Y (2011) Influence of thermal and mechanical cracks on permeability and elastic wave velocities in a basalt from Mt. Etna volcano subjected to elevated pressure. *Tectonophysics* 503:60–74. <https://doi.org/10.1016/j.tecto.2010.09.028>
- Glover PWJ, Gómez JB, Meredith PG (2000) Fracturing in saturated rocks undergoing triaxial deformation using complex electrical conductivity measurements: experimental study. *Earth Planet Sci Lett* 183:201–213. [https://doi.org/10.1016/S0012-821X\(00\)00267-3](https://doi.org/10.1016/S0012-821X(00)00267-3)
- Guéguen Y, Dienes J (1989) Transport properties of rocks from statistics and percolation. *Math Geol* 21:1–13. <https://doi.org/10.1007/BF00897237>
- Guéguen Y, Palciauskas V (1994) Introduction to the physics of rocks. Princeton University Press, Beijing
- Hadley K (1975) V_p/V_s anomalies in dilatant rock samples. *Pure Appl Geophys* 113:1–23. https://doi.org/10.1007/978-3-0348-5534-1_1
- Jordan T, Chen YT, Gasparini P, Madariaga R, Main I, Marzocchi W, Papadopoulos G, Sobolev G, Yamaoka K, Zschau J (2011) Operational earthquake forecasting: State of knowledge and guidelines for utilization. *Annu Geophys* 54:316–391. <https://doi.org/10.4401/ag-5350>
- Kachanov M (1994) Elastic solids with many cracks and related problems. In: Hutchinson JW, Wu TY (eds) *Advances in applied mechanics*. Elsevier, Amsterdam
- Lockner DA, Walsh JB, Byerlee JD (1977) Changes in seismic velocity and attenuation during deformation of granite. *J Geophys Res* 82:5374–5378. <https://doi.org/10.1029/JB082i033p05374>
- Minami T, Utsugi M, Utada H, Kagiyama T, Inoue H (2018) Temporal variation in the resistivity structure of the first Nakadake crater, Aso volcano, Japan, during the magmatic eruptions from November 2014 to May 2015, as inferred by the ACTIVE electromagnetic monitoring system. *Earth Planets Space* 70:138. <https://doi.org/10.1186/s40623-018-0909-2>
- Mitchell TM, Faulkner DR (2008) Experimental measurements of permeability evolution during triaxial compression of initially intact crystalline rocks and implications for fluid flow in fault zones. *J Geophys Res*. <https://doi.org/10.1029/2008JB005588>
- Muñoz G, Bauer K, Moeck I, Schulze A, Ritter O (2010) Exploring the Groß Schönebeck (Germany) geothermal site using a statistical joint interpretation of magnetotelluric and seismic tomography models. *Geothermics* 39:35–45. <https://doi.org/10.1016/j.geothermics.2009.12.004>
- Nimiya H, Ikeda T, Tsuji T (2017) Spatial and temporal seismic velocity changes on Kyushu Island during the 2016 Kumamoto earthquake. *Sci Adv* 3:e1700813. <https://doi.org/10.1126/sciadv.1700813>
- O'Connell RJ, Budiandy B (1974) Seismic velocities in dry and saturated cracked solids. *J Geophys Res* 79:5412–5426. <https://doi.org/10.1029/JB079i035p05412>
- Paterson MS, Wong TF (2005) *Experimental rock deformation—the brittle field*. Springer, Berlin
- Revil A, Cathles LM, Losh S (1998) Electrical conductivity in shaly sands with geophysical applications. *J Geophys Res* 103:23925–23936. <https://doi.org/10.1029/98JB02125>
- Sawayama K, Katayama I (2016) Effects of confining pressure and pore water pressure on the strain behavior and deformation property of Aji granite under triaxial compression test. *J Geol Soc Japan* 122:603–615. <https://doi.org/10.5575/geosoc.2016.0041>
- Scholz CH, Sykes LR, Aggarwal YP (1973) Earthquakes prediction: a physical basis. *Science* 181:803–810. <https://doi.org/10.1126/science.181.4102.803>
- Schubnel A, Nishizawa O, Masuda K, Lei XJ, Xue Z, Guéguen Y (2003) Velocity measurements and crack density determination during wet triaxial experiments on Oshima and Toki granites. *Pure Appl Geophys* 160:869–887. https://doi.org/10.1007/978-3-0348-8083-1_5
- Tomecka-Suchon S, Rummel F (1992) Fracture-induced resistivity changes in granite. *Int J Rock Mech Min Sci* 29:583–587. [https://doi.org/10.1016/0148-9062\(92\)91616-D](https://doi.org/10.1016/0148-9062(92)91616-D)
- Violay M, Heap MJ, Acosta M, Madonna C (2017) Porosity evolution at the brittle-ductile transition in the continental crust: Implications for deep hydro-geothermal circulation. *Sci Rep* 7:7705. <https://doi.org/10.1038/s41598-017-08108-5>
- Walsh JB, Brace WF (1984) The effect of pressure on porosity and the transport properties of rock. *J Geophys Res* 89:9425–9431. <https://doi.org/10.1029/JB089iB11p09425>
- Watanabe T, Higuchi A (2015) Simultaneous measurements of elastic wave velocities and electrical conductivity in a brine-saturated granitic rock under confining pressures and their implication for interpretation of geophysical observations. *Prog Earth Planet Sci* 2:37. <https://doi.org/10.1186/s40645-015-0067-0>
- Zaima K, Katayama I (2018) Evolution of elastic wave velocities and amplitudes during triaxial deformation of Aji granite under dry and water-saturated conditions. *J Geophys Res* 123:9601–9614. <https://doi.org/10.1029/2018JB016377>

Publisher's Note

Springer Nature remains neutral with regard to jurisdictional claims in published maps and institutional affiliations.

Submit your manuscript to a SpringerOpen[®] journal and benefit from:

- Convenient online submission
- Rigorous peer review
- Open access: articles freely available online
- High visibility within the field
- Retaining the copyright to your article

Submit your next manuscript at ► [springeropen.com](https://www.springeropen.com)